Indoor Millimeter Wave MIMO: Feasibility and Performance

Eric Torkildson, Upamanyu Madhow, *Fellow, IEEE,* and Mark Rodwell, *Fellow, IEEE*

***Abstract*—In this paper, we investigate spatial multiplexing at millimeter (mm) wave carrier frequencies for short-range indoor applications by quantifying fundamental limits in line-of-sight (LOS) environments and then investigating performance in the presence of multipath and LOS blockage. Our contributions are summarized as follows. For linear arrays with constrained form factor, an asymptotic analysis based on the properties of prolate spheroidal wave functions shows that a sparse array producing a spatially uncorrelated channel matrix effectively provides the maximum number of spatial degrees of freedom in a LOS environment, although substantial beamforming gains can be obtained by using denser arrays. This motivates our proposed mm-wave MIMO architecture, which utilizes arrays of subarrays to provide both directivity and spatial multiplexing gains. System performance is evaluated in a simulated indoor environment using a ray-tracing model that incorporates multipath effects and potential LOS blockage. Eigenmode transmission with waterfilling power allocation serves as a performance benchmark, and is compared to the simpler scheme of beamsteering transmission with MMSE reception and a fixed signal constellation. Our numerical results provide insight into the spatial variations of attainable capacity within a room, and the combinations of beamsteering and spatial multiplexing used in different scenarios.**

***Index Terms*—Millimeter wave communication, MIMO, channel capacity, antenna arrays.**

I. Introduction

THE demand for faster data rates, combined with recent advances in low cost silicon CMOS and silicon germanium mm-wave integrated circuits [1], has generated significant interest in designing multigigabit wireless links that utilize the 7 GHz of unlicensed spectrum surrounding 60 GHz. Standardization efforts include the recently published IEEE 802.15.3c-2009 [2] and ECMA-387 [3] standards, as well as emerging industry-backed specifications such as WiGig [4] and WirelessHD [5]. Multigigabit wireless data rates will facilitate applications such high definition (HD) multimedia transmission and high-speed data sync. In this paper, we propose increasing mm-wave data rates further by employing multiple-input, multiple-output (MIMO) spatial processing techniques.

MIMO links transmit and receive multiple independent data streams in parallel through spatial multiplexing, which increases data rates without an accompanying increase in bandwidth or transmit power [6] [7]. Since its introduction, spatial multiplexing has drawn considerable attention in the literature and has seen inclusion in standards and commercial products in both cellular and wireless local area networks operating at lower carrier frequencies. While lower-frequency systems typically rely on rich multipath to enable spatial multiplexing, the small carrier wavelength at 60 GHz implies that spatial multiplexing gains are available even in LOS environments with moderate antenna separation, as has been demonstrated in recent hardware prototypes [8] [9]. In this paper, we investigate the feasibility and effect of spatial multiplexing for indoor point-to-point mm-wave links, where the nodes employ antenna arrays that have form factors consistent with typical consumer electronic devices (e.g. laptops, set-top boxes, televisions, etc.).

Contributions: Our main contributions are summarized as follows. While it is well known that suitably choosing antenna spacing produces orthogonal eigenmodes for LOS spatial multiplexing, we show here, for the example of linear arrays, that this strategy is effectively optimal in terms of maximizing the number of degrees of freedom for a given array length. Our analysis is based on the limit of a continuous linear array, where the channel spatial eigenmodes are prolate spheroidal waveforms, analogous to the classical analysis of time- and band-limited systems. We then evaluate the performance of an array of subarrays architecture, where the subarrays provide beamsteering gains, and are spaced to provide spatial multiplexing gains with eigenmodes which are orthogonal for a LOS link at a nominal range. We evaluate its performance in the sparse multipath environment resulting from highly directive transmissions using geometrical optics (i.e., ray tracing) to model the channel, with a view to quantifying variations in performance with the relative location of transmitter and receiver, and with LOS blockage. We compare a waterfilling benchmark against a strategy with independent transmit beamsteering for each subarray, together with linear MMSE spatial interference suppression at the receiver. Our numerical results provide insight into how the spatial eigenmodes and the achievable capacity vary with the propagation environment. We conclude that the spatial multiplexing gain provided by our architecture is robust to LOS blockage and to variations in the locations of the transmitter and receiver within the room, while requiring a reasonably small power per transmit element realizable by low-cost CMOS processes.

Related Work: The number of spatial degrees of freedom of a MIMO channel given array aperture constraints was previously evaluated in [10] in the context of a scattering envi-

Manuscript received October 18, 2010; revised May 4, 2011; accepted August 13, 2011. The associate editor coordinating the review of this paper and approving it for publication was A. Molisch.

The authors are with the Department of Electrical and Computer Engineering, University of California, Santa Barbara, CA 93106 USA (e-mail: etorkild@ece.ucsb.edu).

This research was supported in part by the National Science Foundation under grant CNS-0832154, and by the Institute for Collaborative Biotechnologies through grant W911NF-09-0001 from the U.S. Army Research Office.

Digital Object Identifier 10.1109/TWC.2011.092911.101843

ronment. Their derivation uses the plane wave approximation, which holds when antenna spacing is small relative to the wavelength, in which case a LOS channel is limited to a single spatial degree of freedom. Our interest here is in antennas with larger antenna spacing (feasible because the wavelength is so small), where purely LOS channels can indeed offer multiple degrees of freedom. The capacity of LOS MIMO channels was previously studied by several authors [11], [12], [13], [14], with a view to identifying the optimal antenna array geometries that maximize the LOS channel capacity. In this paper, we show that such geometries are indeed near-optimal in terms of degrees of freedom maximization, given a constraint on the node form factor. The validity of the ray-tracing approach used in our performance evaluation is supported by measurement studies at at 60 GHz such as [15] that observe sparse multipath environments. The capacity of multi-antenna mm-wave links was previously studied in [16] using a similar propagation model to ours, but practical array of subarrays transceiver architectures (validated by our study of fundamental limits) were not considered. We have previously studied array of subarrays architectures in the context of outdoor mm-wave links [17], but the issue investigated there is the effect of range mismatch [18] rather than multipath and LOS blockage. Working prototypes demonstrating LOS mm-wave MIMO are reported in [8] [9].

The paper is organized as follows. In Section II, we review the array geometry criterion that guarantees an orthogonal channel matrix for LOS MIMO. We then show that this is near-optimal by deriving a limit on the number of spatial degrees of freedom with array length (i.e. form factor) constraints. A system architecture that provides array gain and spatial multiplexing gain is introduced in Section III. An indoor environment modeled using ray-tracing techniques is described in Section IV. In Section V, the performance of the proposed architecture is evaluated in terms of channel capacity under LOS and non-LOS (NLOS) conditions. Conclusions are discussed in Section VI.

II. Fundamental Limits of LOS MIMO

In this section, we derive limits on the number of spatial degrees of freedom of a LOS MIMO channel given array length constraints. We find that the form factors of typical consumer electronics devices are sufficient to allow multiple degrees of freedom.

A. LOS MIMO Channel Model

Consider a link consisting of two N-element arrays. Assuming a flat-fading MIMO channel, the received signal vector $\mathbf{y} \in \mathbb{C}^{N\times 1}$ is given by

$$\mathbf{y} = \mathbf{H}\mathbf{x} + \mathbf{w}, \tag{1}$$

where $\mathbf{x} \in \mathbb{C}^{N\times 1}$ is the transmitted signal vector, $\mathbf{H} \in \mathbb{C}^{N\times N}$ is the channel matrix, $\mathbf{w} \in \mathbb{C}^{N\times 1}$ is additive complex white Gaussian noise with with covariance $N_0\mathbf{I}_N$, and $\mathbf{I}_N$ is the $N \times N$ identity matrix. In a purely LOS channel, the complex channel gain $h_{m,n}$, representing the (m,n)th element of $\mathbf{H}$, can be modeled as

$$h_{m,n} = \frac{\lambda}{4\pi p_{m,n}} \exp\left(-j\frac{2\pi}{\lambda}p_{m,n}\right), \tag{2}$$

where λ is the carrier wavelength and $p_{m,n}$ is the path length from the nth transmit antenna to the mth receive antenna.

Assuming the arrays are uniformly-spaced and aligned broadside, the path length is given by $p_{m,n} = \sqrt{R^2 - (md_T - nd_R)^2}$, where R is the link range, and d_R and d_T denote the distance between neighboring receive antennas and transmit antennas, respectively. When R is much larger than the length of either array, we can approximate the path length by $p_{m,n} \approx R + (md_t - nd_r)^2/(2R)$. The channel gain is then

$$h_{m,n} \approx \frac{\lambda}{4\pi R} \exp\left(-j\frac{2\pi}{\lambda}\left(R + \frac{(md_T - nd_R)^2}{2R}\right)\right). \tag{3}$$

In contrast to a NLOS MIMO channel, which is highly dependent on the surrounding multipath scattering environment, we note that the LOS MIMO channel is specified by the carrier frequency and the relative positions of the array elements. We proceed to review results that show that a high-rank LOS MIMO channel is produced if the spacing between adjacent elements is chosen appropriately.

B. Optimally Spaced Arrays

Let us first consider a setting in which the number of transmit and receive elements (rather than the array length) is fixed, and the goal is to determine the optimal spacing between the elements. In the moderate to high signal-to-noise ratio (SNR) regime, the Shannon capacity of an $N \times N$ MIMO channel is maximized when the N singular values of the associated channel matrix are equal. This is achieved when the columns of $\mathbf{H}$ are orthogonal, i.e. the receiver's array response to a given transmit element is orthogonal to its response to any other transmit element. Denoting the ith column of $\mathbf{H}$ by $\mathbf{h}_{*i}$, the inner product between the kth and lth column is given by

$$\begin{aligned}\langle \mathbf{h}_{*k}, \mathbf{h}_{*l}\rangle &= \left(\frac{\lambda}{4\pi R}\right)^2 \sum_{m=0}^{N-1} e^{j\frac{2\pi}{\lambda}(p_{m,k}-p_{m,l})} \\ &= \left(\frac{\lambda}{4\pi R}\right)^2 \sum_{m=0}^{N-1} e^{j\frac{2\pi}{\lambda R}md_Td_R(l-k)} \\ &= \left(\frac{\lambda}{4\pi R}\right)^2 \frac{\sin(\pi N(l-k)\frac{d_Td_R}{\lambda R})}{\sin(\pi(l-k)\frac{d_Td_R}{\lambda R})},\end{aligned} \tag{4}$$

where the channel gains are given by (3). The inner product is driven to zero when the following condition is satisfied

$$d_Td_R = \frac{R\lambda}{N}. \tag{5}$$

When this condition holds, $\mathbf{H}$ is a scaled unitary matrix with equal singular values, which we denote by σ_n for $n = 1, \ldots, N$. Each non-zero singular value corresponds to an eigenmode (or eigenchannel) over which data can be transmitted. We refer to a pair of arrays satisfying (5) as *optimally spaced* ULAs. This orthogonality condition was originally derived in [11], and equivalent conditions have since been derived for broadside aligned uniform rectangular arrays (URAs) [13], as well as arbitrarily aligned ULAs [14] and URAs [19].

Now, if the lengths of the transmit and receive arrays are constrained and N is arbitrary, we can determine from (5) the

maximum number of antennas that can be supported while preserving the orthogonality condition. Noting that the length of a ULA is given by $L = d(N-1)$, where d is the interelement spacing, and solving (5) for N, the maximum number of antennas is given by

$$N_U = \lfloor 1 + \frac{L_T L_R}{2\lambda R} + \frac{1}{2}\sqrt{\left(2 + \frac{L_T L_R}{\lambda R}\right)^2 - 4} \rfloor, \quad (6)$$

where L_T is the maximum transmit array length, L_R is the maximum receive array length, and $\lfloor a \rfloor$ is the largest integer less than or equal to a.

Equation (6) specifies the maximum number of spatial degrees of freedom available to a LOS MIMO link while satisfying both the orthogonality condition and a set of array length constraints. Such a design may be termed an *optimally spaced sparse array,* where the sparsity is required for orthogonality. In the next section, we investigate what can be gained by forgoing orthogonality and increasing the antenna count of our fixed-length arrays beyond N_U.

C. Spatial Degrees of Freedom

Equation (6) specifies the maximum number of spatial degrees of freedom available to a LOS MIMO link while satisfying both the orthogonality condition and a set of array length constraints. We may ask what can be gained by forgoing orthogonality and increasing the antenna count of our fixed-length arrays beyond N_U. We first consider two LOS MIMO links as an example. The first link uses optimally spaced arrays, with $N = 8$, $\lambda = 5$ mm, $R = 5$ m, and $L_T = L_R = 39.1$ cm. The squared singular values the associated channel matrix, plotted in Fig. 1, are of equal value, as expected. The arrays of the second link also have lengths of 39.1 cm, but the number of uniformly spaced elements is increased fourfold to $N = 32$. Fig. 1 plots the largest twelve squared singular values. We observe that the additional antennas provide mostly power gains to the first eight eigenchannels rather than degree of freedom gains. The additional eigenvalues are significantly weaker and drop off rapidly to zero.

To see whether this result continues to hold for larger N, we take the limit as N approaches infinity. Based on our observation of Fig. 1, namely that additional antennas seem to yield primarily array processing gains to the first N_U eigenmodes, we may expect the squared singular values to increase in proportion to N^2. This follows from the fact that, under a transmit power constraint, transmit beamforming and receive beamforming each provide a factor of N power gain. We therefore introduce a normalized form of the channel matrix given by

$$\tilde{\mathbf{H}} = \frac{4\pi R}{\lambda N}\mathbf{H}, \quad (7)$$

where the $1/N$ scaling factor normalizes the squared singular values by $1/N^2$. With this choice of normalization, $\sum_{n=1}^{N} \tilde{\sigma}_n^2 = 1$, where $\tilde{\sigma}_n$ are the singular values of $\tilde{\mathbf{H}}$. Substituting $\tilde{\mathbf{H}}$ for $\mathbf{H}$ in (1) and disregarding additive noise, the signal at the kth receive antenna is given by

$$y_k = \frac{1}{N}\sum_{m=0}^{N} \exp\left(-j\frac{2\pi}{\lambda}\left(R + \frac{(md_T - nd_R)^2}{2R}\right)\right) x_m. \quad (8)$$

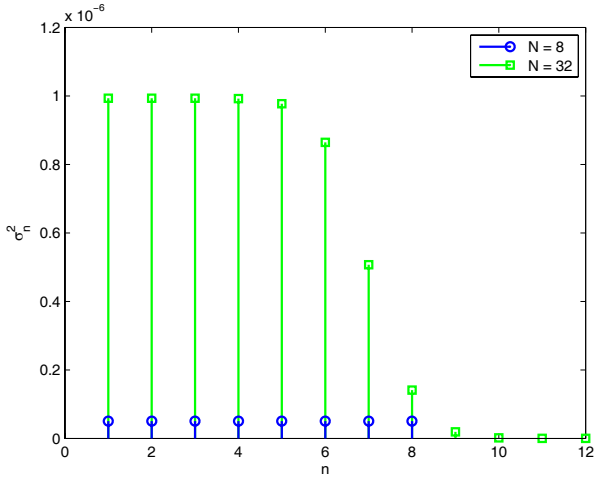

Fig. 1. Squared singular values of $\mathbf{H}$ for $N = 8$ (optimally spaced) and $N = 32$, assuming $f_c = 60$ GHz, $R = 5$ m, and $L_T = L_R = 39.1$ cm.

In the limit as N goes to infinity and the interelement spacing becomes infinitesimal, we can express the received signal at point $p \in [-L_R/2, L_R/2]$ on the receive array as

$$y(p) = \frac{1}{L_T} e^{-j\frac{2\pi}{\lambda}R} \int_{-L_T/2}^{L_T/2} e^{-j\frac{2\pi}{\lambda}\frac{(q-p)^2}{2R}} x(q)dq, \quad (9)$$

where $x(q)$ is the transmitted signal at point $q \in [-L_T/2, L_T/2]$ on the transmit array.

The integral kernel

$$G(p,q) = \frac{e^{-j\frac{2\pi}{\lambda}R}}{L_T} e^{-j\frac{2\pi}{\lambda}\frac{(q-p)^2}{2R}}. \quad (10)$$

was previously studied in the context of the diffraction limited optics by Thaning *et al.* in [20], and the analysis here follows their approach. Equation (10) can be expanded via the spectral theorem as

$$G(p,q) = \sum_{n=1}^{\infty} g_n a_n^*(q) b_n(p), \quad (11)$$

where g_n and $a_n(q)$ are the eigenvalues and eigenfunctions of the integral equation

$$|g_n|^2 a_n(q) = \int_{-L_T/2}^{L_T/2} K(q', q) a_n(q') dq', \quad (12)$$

and where

$$K(q', q) = \int_{-L_R/2}^{L_R/2} G^*(p, q) G(p, q') dp. \quad (13)$$

The functions $b_n(p)$ are defined by

$$g_n b_n(p) = \int_{-L_T/2}^{L_T/2} G(p,q) a_n(q) dq.$$

The functions $a_n(q)$, which are ordered such that $|g_1| \geq |g_2| \geq \ldots \geq |g_n|$, form an orthonormal set over the interval $[-L_T/2, L_T/2]$, and hence the received signal can be expressed as

$$y(p) = \sum_{n=1}^{\infty} A_n b_n(q), \quad (14)$$

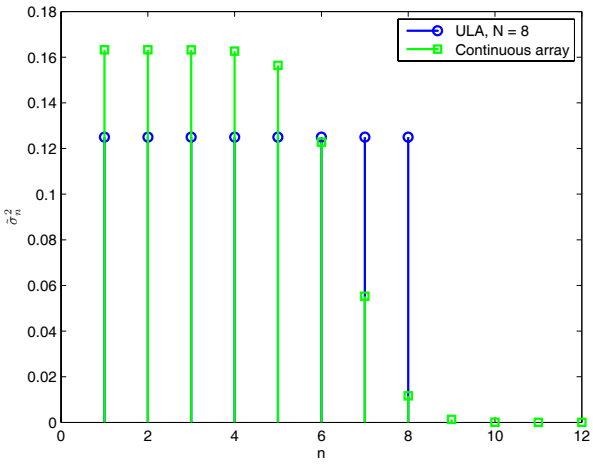

Fig. 2. The first twelve eigenvalues of the continuous array channel with $f_c = 60$ GHz, $R = 5$ m, and $L_T = L_R = 39.1$ cm. Also shown are the squared singular values of the normalized ULA channel with $N = 8$.

where

$$A_n = g_n \int_{-L_T/2}^{L_T/2} a_n^*(p_T) x(p_T) dp_T.$$

Expressing the eigenfunctions in the form

$$a_n(q) = \exp\left(i\frac{2\pi}{\lambda}\frac{q^2}{2R}\right)\alpha_n(q), \tag{15}$$

we can substitute (15) and (13) into (12) to obtain the following equation

$$\frac{L_T^2}{\lambda R}|g_n|^2\alpha_n(q) = \int_{-L_T/2}^{L_T/2} \frac{\sin 2\pi W(q-q')}{\pi(q-q')}\alpha_n(q')dq', \tag{16}$$

where $W = L_R/(2\lambda R)$. The integral equation (16) defines a set of prolate spheroidal wavefunctions (PSWFs), a family of functions investigated extensively by Slepian et al. in the context of bandlimited and approximately time-limited signals [21] [22]. The eigenvalues $|g_n|^2$ are related to v_n, the eigenvalues of the PSWFs, by $|g_n|^2 = v_n \lambda R/L_T^2$. A well-known property of the PSWFs is that their eigenvalues remain approximately equal to one until n nears a critical value, given here by

$$S = 2WL_T = \frac{L_T L_R}{\lambda R}, \tag{17}$$

after which they drop off rapidly to zero. Correspondingly, A_n drops off to zero for $n > S$, and the received signal $y(p)$ is specified to a high degree of accuracy by the first $S+1$ values of A_n. We conclude that the number of degrees of freedom of the continuous array link is limited to approximately

$$N_C = \frac{L_T L_R}{\lambda R} + 1. \tag{18}$$

We note that $N_C \approx N_U$, although as a result of factoring out the beamforming gain, N_C is generally a more conservative estimate of the degrees of freedom.

Fig. 2 plots the first twelve eigenvalues of the continuous array channel, $|g_n|^2$ for $n = 1, \ldots, 12$, when $R = 5$ m, and $L_T = L_R = 39.1$ cm. Their transition to zero is centered around $S = 6.125$, in agreement with (17). Comparing Fig. 2 and Fig. 1, we find that squared singular values of the $N = 32$ ULA link are approximately proportional to the continuous array eigenvalues.

Relating the the PSWF results to discrete ULAs, we observe that for large N, the squared singular value σ_n^2 increases by an amount proportional to $|g_n|^2$ when an additional element is added to the array. Thus $\{|g_n|^2\}$ describes how the power gain provided by an additional antenna is distributed among the eigenchannels of a ULA link when $N \gg N_U$.

The preceding asymptotic analysis yields fairly specific guidelines for transceiver design. First, increasing antenna count beyond the optimally spaced sparse design is an impractical means of increasing the number of degrees of freedom: while the power gain may be sufficient that more than N_U eigenchannels are utilized under a given power allocation scheme, these modes will remain significantly weaker than the dominant modes. Indeed, for the form factors and ranges of interest for indoor mm-wave MIMO, the number of dominant modes is already quite large. However, while optimally spaced sparse arrays are, in fact, near-optimal in the number of spatial degrees of freedom they provide, our analysis also indicates that the SNR per degree of freedom can be significantly improved by increasing the number of elements. This observation motivates the array of subarrays architecture presented in the following section.

III. LOS mm-Wave MIMO Architecture

Our proposed MIMO transceiver architecture in Fig. 3 is based on the preceding optimal spacing criterion given by (5). N independent data streams are precoded and transmitted over an N-element ULA, where the spacing d is chosen to satisfy (5) given an expected link range R_o. Each element of the ULA is a square $\lambda/2$-spaced subarray, which can be implemented as a monolithic millimeter wave integrated circuit. Because the spacing between subarray elements is small, the subarrays provide array gain rather than spatial multiplexing gain. The additional directivity helps to offset propagation loss at mm-wave frequencies and attenuate multipath. Each subarray is an $M \times M$ square array, so the total number of antennas per node is given by $N_T = NM^2$. The receiver consists of an identical array-of-subarrays structure, with received signals feeding into a equalizer designed to null spatial interference. We now describe two spatial equalization and modulation schemes based on the above architecture.

A. Waterfilling Benchmark

Our performance benchmark is standard waterfilling based eigenmode transmission. This employs a transmit precoder and a receive spatial equalizer based on the singular value decomposition (SVD) of the channel matrix $\mathbf{H}$, such that the channel is decomposed into N non-interfering parallel subchannels, or eigenmodes. The SVD of the channel matrix $\mathbf{H}$ is given by

$$\mathbf{H} = \mathbf{U}\mathbf{\Sigma}\mathbf{V}^{\mathbf{H}},$$

where $\mathbf{U}, \mathbf{V} \in \mathbb{C}^{N_T \times N_T}$ are unitary and $\mathbf{\Sigma} \in \mathbb{R}^{N_T \times N_T}$ is a diagonal matrix whose nonzero entries are the ordered singular values of $\mathbf{H}$, given by $\sigma_1 \geq \sigma_2 \geq \ldots \geq \sigma_{N_T}$. Let $\mathbf{V}_N$ and

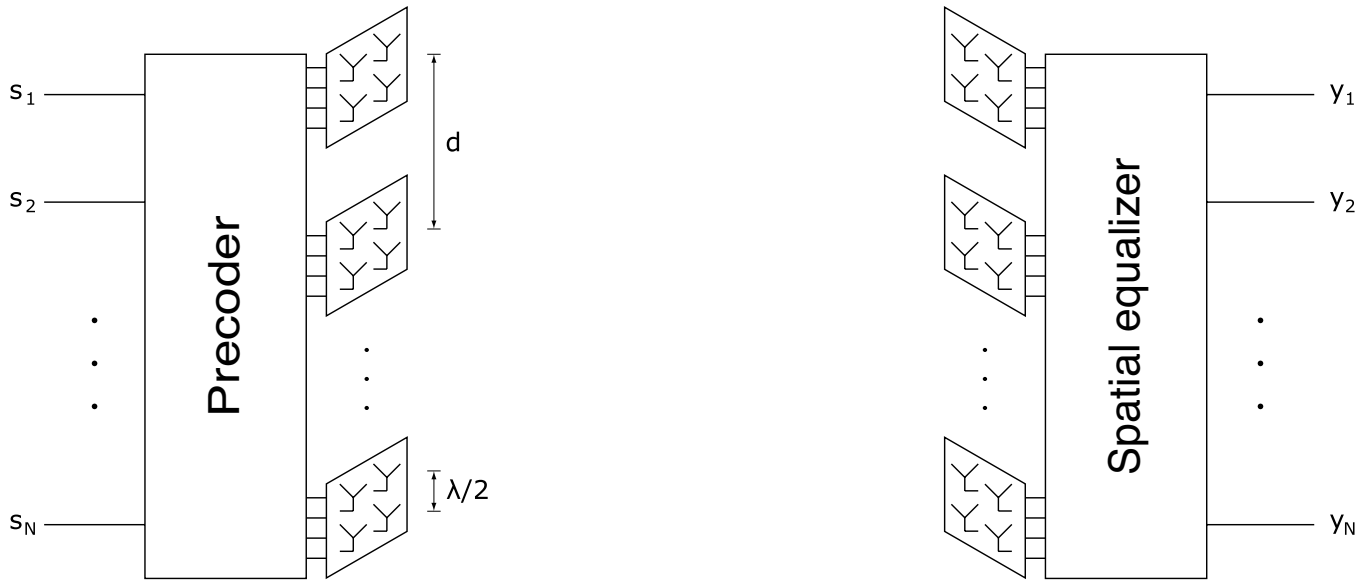

Fig. 3. Proposed millimeter wave MIMO architecture. Each node possesses a linear array of N $\lambda/2$-spaced uniform square subarrays, which provide additional directivity to offset increased propagation loss at millimeter wave frequencies.

$\mathbf{U}_N$ denote the matrices composed of the first N columns of $\mathbf{V}$ and $\mathbf{U}$, respectively. The data vector $\mathbf{s}$ is premultiplied by $\mathbf{V}_N$ at the transmit precoder stage and the received data $\mathbf{r}$ is filtered by $\mathbf{U}_N^H$, resulting in

$$\mathbf{y} = \mathbf{U}_N^H \mathbf{r} = \mathbf{U}_N^H(\mathbf{H}\mathbf{V}_N\mathbf{s} + \mathbf{w}) = \mathbf{\Sigma}_N\mathbf{s} + \tilde{\mathbf{w}},$$

where $\mathbf{\Sigma}_N$ is the $N \times N$ submatrix consisting of the first N columns and N rows of $\mathbf{\Sigma}$. Note that the distribution of the noise component remains unchanged because the columns of $\mathbf{U}_N$ are orthonormal. Effectively, the channel is decomposed into N parallel subchannels of the form

$$y_i = \sigma_i s_i + \tilde{w}_i \quad i = 1, 2, \ldots, N.$$

The channel capacity, given by

$$C = \sum_i^N \left(\log \frac{\mu\sigma_i^2}{N_0} \right)^+, \tag{19}$$

is achieved when the input symbols s_i are Gaussian distributed and the power allocated to the ith channel, denoted by $P_i = E[|s_i|^2]$, obeys the waterfilling power allocation policy. P_i is given by

$$P_i = \left(\mu - \frac{N_0}{\sigma_i^2} \right)^+, \tag{20}$$

where a^+ indicates $\max\{0, a\}$, the value of μ is chosen such that $\sum_i P_i = P_T$, and P_T is a total power constraint. If $(\mu - N_0/\sigma_i^2) < 0$, no power or data is allocated to the ith eigenchannel.

B. Transmit Beamsteering/Receive MMSE

While the previous scheme provides an upper bound on link performance, it is important to identify more conservative performance estimates that represent typical hardware and signal processing constraints. To this end, we consider a scheme in which the transmitter sends a single data stream from each subarray, with each subarray limited to beamsteering in a given direction. We assume the transmitter knows the directions of the LOS and first-order reflection paths to the receiver (these can be learned by scanning at start-up), and beamsteering is constrained along these paths. From this set of paths, the transmitter beamsteers in the direction(s) that maximize the sum-rate spectral efficiency. The constellation per data stream is fixed (we use 16QAM in our numerical results). The spatially multiplexed data streams can now interfere with each other, and we employ linear MMSE spatial interference suppression to separate them out at the receiver.

Note that, as demonstrated in recent hardware prototypes [8], spatial processing (e.g., linear interference suppression) for a quasi-static channel can be handled in our architecture on a slow time scale using (digitally controlled) analog processing, thus avoiding the need for high-speed analog-to-digital converters (ADCs) with large dynamic range. Digitization can then be performed with ADCs with lower dynamic range after separation of the multiplexed data streams.

The beamsteering weight applied to the antenna in the kth column and lth row of the jth subarray is given by

$$a_{jkl} = \exp\left(-i\pi\left((k-1)\cos\theta_j \sin\phi_j + (l-1)\cos\phi_j\right)\right) \quad k, l \in \{1, 2, \ldots, M\}, \tag{21}$$

where θ_j and ϕ_j are the azimuthal and polar steering angles, respectively. Let a_{jkl} be the (k,l)th entry of the $M \times M$ matrix $\mathbf{A}(\theta_j, \phi_j)$ and let $\mathbf{a}(\theta_j, \phi_j) = \mathrm{vec}\,(\mathbf{A}(\theta_j, \phi_j))$ be the vector formed from concatenating the columns of $\mathbf{A}(\theta_j, \phi_j)$. The precoding matrix $\mathbf{G}$ is given by

$$\mathbf{G} = \frac{1}{M} \begin{pmatrix} \mathbf{a}(\theta_1, \phi_1) & \mathbf{0} & \cdots & \mathbf{0} \\ \mathbf{0} & \mathbf{a}(\theta_2, \phi_2) & \cdots & \vdots \\ \vdots & \vdots & \ddots & \mathbf{0} \\ \mathbf{0} & \cdots & \mathbf{0} & \mathbf{a}(\theta_N, \phi_N) \end{pmatrix}, \tag{22}$$

where $\mathbf{0}$ is an $M^2 \times 1$ vector of zeros.

At the receiver, full channel state information is assumed. The input to the spatial equalizer is given by

$$\mathbf{r} = \mathbf{HGs} + \mathbf{w} = \hat{\mathbf{H}}\mathbf{s} + \mathbf{w}, \tag{23}$$

where $\mathbf{s}$ is the $N \times 1$ data vector, $\mathbf{G}$ is the $NM^2 \times N$ steering matrix, and $\hat{\mathbf{H}} = \mathbf{HG}$ is an $NM^2 \times N$ equivalent channel matrix combining the propagation environment and the steering matrix. We now assume equal power allocation across data streams, such that $E[|s_i|^2] = P_T/N$. The equalizer output is given by

$$\mathbf{y} = \mathbf{C}^H\mathbf{r} = \mathbf{C}^H\left(\hat{\mathbf{H}}\mathbf{s} + \mathbf{w}\right), \tag{24}$$

where equalizer coefficients are specified by $\mathbf{C}$. The coefficients of the MMSE equalizer are given by

$$\mathbf{C}_{\mathrm{MMSE}} = \left(\frac{P_T}{N}\hat{\mathbf{H}}\hat{\mathbf{H}}^H + P_N\mathbf{I}_{NM^2}\right)^{-1}\frac{P_T}{N}\hat{\mathbf{H}}, \tag{25}$$

where $P_N = N_0B$ is the noise power and B is the bandwidth.

The signal to interference and noise ratio (SINR) at the kth output of the equalizer is given by

$$\gamma_k = \frac{\frac{P_T}{N}|\mathbf{c}_k^H\hat{\mathbf{H}}_k|^2}{\frac{P_T}{N}\sum_{j\neq k}|\mathbf{c}_j^H\hat{\mathbf{H}}_k|^2 + P_N\mathbf{c}_k^H\mathbf{c}_k}, \tag{26}$$

where $\mathbf{c}_k$ is the kth column of $\mathbf{C}_{\mathrm{MMSE}}$. The spectral efficiency is computed with the interference treated as Gaussian noise, and with the symbol constellation restricted to 16-QAM.

IV. Indoor Propagation Model

The optimal antenna spacing criterion given by (5) assumes the transmit and receive arrays are aligned parallel, the channel is purely LOS, and the link range is known *a priori*. For practical indoor applications, none of these assumptions can be expected to hold, and we wish to evaluate the performance of the proposed architecture when operating under more realistic scenarios. To this end, we present a indoor environment propagation model that allows us to assess the impact of multipath propagation, link range variations, and LOS blockage.

The propagation environment, shown in Fig. 4, is a room of dimensions 5 m $\times$ 5 m $\times$ 3 m. The receive array lies horizontally along the plane of the front wall, centered at coordinates $(2.5\ \mathrm{m}, 0, 1.5\ \mathrm{m})$. The transmitter's position is variable, and given by coordinates $(x, y, 1.5\ \mathrm{m})$, where $0 \leq x \leq 5$ m and $0 \leq y \leq 5$ m. Unless otherwise noted, the transmit array is also aligned parallel with the front wall.

Given the specular nature of mm-wave reflections, we model the environment using the method of geometrical optics [23]. The LOS paths from transmitter to receiver, as well as single-bounce and double-bounce reflected paths off the side walls and ceiling, contribute to the channel matrix $\mathbf{H}$. Higher order reflections are disregarded in the simulations due to the additional path losses and reflection losses they incur, as well as the directivity provided by the subarrays. The channel matrix $\mathbf{H} \in \mathbb{C}^{N_T \times N_T}$ can be written

$$\mathbf{H} = \mathbf{H}_{\mathrm{LOS}} + \sum_{j=1}^{3}\mathbf{H}_{\mathrm{R1},j} + \sum_{k=1}^{4}\mathbf{H}_{\mathrm{R2},k}, \tag{27}$$

where $\mathbf{H}_{\mathrm{LOS}}$ is the LOS component, $\{\mathbf{H}_{\mathrm{R1},j}\}$ are the three first-order reflected path components off the right wall, left wall, and ceiling, and $\{\mathbf{H}_{\mathrm{R2},k}\}$ are the second-order reflections, which include two second-order reflections off both side walls, and two second-order reflections off a combination of a side wall and the ceiling. The (m,n)th entry of $\mathbf{H}_{\mathrm{LOS}}$ is given by

$$h_{\mathrm{LOS}}(m,n) = \frac{\lambda}{4\pi p_{\mathrm{LOS}}(m,n)}e^{-i\frac{2\pi}{\lambda}p_{\mathrm{LOS}}(m,n)}. \tag{28}$$

The (m,n)th entry of $\mathbf{H}_{\mathrm{R1},j}$ is given by

$$h_{\mathrm{R1,j}}(m,n) = \Gamma(\theta_{\mathrm{R1,j}})\frac{\lambda}{4\pi p_{\mathrm{R1,j}}(m,n)}e^{-i\frac{2\pi}{\lambda}p_{\mathrm{R1,j}}(m,n)}, \tag{29}$$

where $p_{\mathrm{R1,j}}(m,n)$ is the length of the path from the nth transmit antenna to the point of reflection to the mth receive antenna, and $\theta_{\mathrm{R1,j}}$ is the reflected ray's angle of incidence. $\Gamma(\theta_{\mathrm{R1,j}})$ is the perpendicular Fresnel reflection coefficient [24] in the case of a wall reflection or the parallel Fresnel reflection coefficient in the case of a ceiling reflection. The (m,n)th entry of $\mathbf{H}_{\mathrm{R2,k}}$ is given by

$$\begin{aligned} h_{\mathrm{R2,k}}(m,n) =& \Gamma_1(\theta_{\mathrm{R2,k}})\Gamma_2(\phi_{\mathrm{R2,k}})\frac{\lambda}{4\pi p_{\mathrm{R2,k}}(m,n)} \\ &\cdot e^{-i\frac{2\pi}{\lambda}p_{\mathrm{R2,j}}(m,n)}, \end{aligned} \tag{30}$$

where $p_{\mathrm{R2,k}}(m,n)$ is the length of the reflected path from the nth transmit antenna to the first point of reflection, then to the second point of reflection, and finally to the mth receive antenna. $\theta_{\mathrm{R2,k}}$ is angle of incidence of the first reflection and $\phi_{\mathrm{R2,k}}$ is the angle of incidence of the second reflection. Γ_1 and Γ_2 are the reflection coefficients for the first and second reflections, respectively. As before, they represent perpendicular or parallel reflection coefficients depending on whether the corresponding reflected surfaces are side walls or the ceiling, respectively. We assume the floor is carpeted, and we hence ignore floor reflections due to the high reflection loss of carpeted surfaces [25].

There are two scenarios where modification of (27) is required. The first is when the LOS is blocked, referred to herein as the non-LOS (NLOS) scenario, which we model by removing the $\mathbf{H}_{\mathrm{LOS}}$ term from (27). The second scenario may occur when we alter the alignment of transmit array.

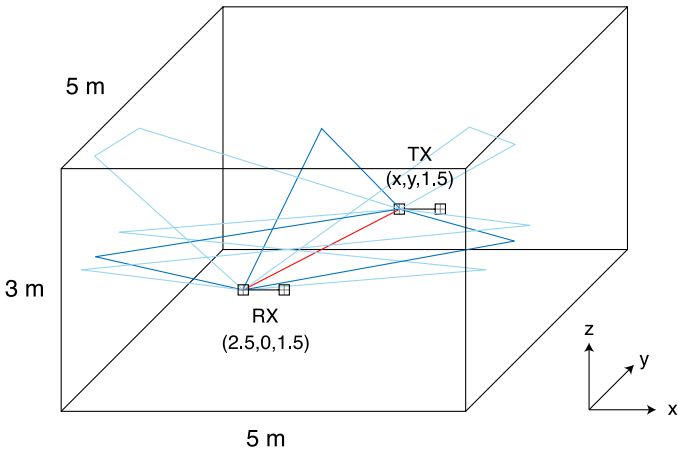

Fig. 4. Indoor environment model showing LOS, first-order reflection, and second-order reflection propagation paths from a transmit subarray element to a receive subarray element.

In particular, if we rotate the array around the vertical axis that passes through its midpoint, a point of reflection on the left or wall may fall behind the array. Since we assume the energy radiated behind the array is highly attenuated by the transmitting device itself, this reflection component is omitted.

V. Results

In this section, we evaluate the spectral efficiency achieved by the mm-wave MIMO architectures proposed in Section III using the indoor propagation model.

System and environment parameters: The room dimensions are 5 m $\times$ 5 m $\times$ 3 m. The spacing between subarrays, given by $d = \sqrt{2.5\lambda/N}$, is chosen such that the LOS component of the channel is spatially uncorrelated when the transmit node is located at the center the room. The link operates at a carrier frequency of 60 GHz, with a corresponding wavelength of $\lambda = 5$ mm. The noise power at the receiver is given by $P_N = kTBF$, where k is the Boltzmann constant, $B = 2.16$ GHz is the bandwidth, $T = 300$ K is the operating temperature, and $F = 10$ dB is the noise figure. The relative dielectric constant $\epsilon_r = 2.8$ and conductivity $\sigma = 0.221$ of the wall and ceiling surfaces are chosen to represent plasterboard [25].

Antenna array model: Our numerical results are for 4×4 $\lambda/2$-spaced square subarrays. The overall array length is then $L = (N-1)d+1.5\lambda$, where N is the number of subarrays, and d the spacing between subarrays. For fixed N and d, spatial multiplexing gains are attained even with smaller 2×2 or 3×3 subarrays, but the smaller beamforming gain provided by each subarray implies that higher transmit power per element must be used to attain results similar to the capacities given below. For instance, if 9-element subarrays are used in place of 16-element subarrays, similar performance can be achieved by increasing the transmit power per element by approximately 8 dBm. For 4-element subarrays, the additional required power is roughly 18 dBm. The individual antenna elements are modeled as isotropic (or more accurately, hemispherical), radiating outward from the plane of the array. Thus, the steering range of the subarrays is $[0°, 180°]$ in the polar and azimuthal directions (where the plane of the subarrays defines the XY plane).

Implementation issues: While the preceding idealized model suffices for our present purpose of providing system-level insights, we briefly discuss some important implementation issues and their implications below.

Feed network losses: The first point to note is that increasing the subarray size indefinitely to get more and more beamforming gain is difficult: larger arrays suffer from higher feed network losses because signals must be routed over longer distances. For an active$M \times M$ subarray with M^2 power amplifiers (transmit) or low noise amplifiers (receive) implemented on an RFIC, signals must be routed over a maximum distance of approximately $l = (M-1)\lambda/2$ from the RFIC to or from the antenna elements. An attenuation of 0.1 dB/mm is fairly typical at 60 GHz [26], so that the feed network loss is less than 1 dB for the 4×4 subarrays considered here (maximum routing length of about 7.5 mm). Thus, feed network losses for our setting are small relative to the 12 dB of beamforming gain provided by the subarray (on either transmit or receive). However, since feed network losses grow exponentially with M, while array gain grows in proportion to M^2, designs for very large arrays (not of interest for the indoor links considered here) would probably require partitioning of RF functionalities among multiple ICs so as to limit the routing length to any given antenna element.

Mutual coupling: Mutual coupling between nearby antenna elements is well known to distort the response of an antenna array, and can be modeled as a matrix transformation of the geometrically computed subarray response. In our setting, coupling across subarrays can be ignored because of the relatively large spacing between them, but inter-element coupling within a subarray implies that the array response for a subarray may differ from the ones that we compute here, which are based on purely geometric considerations. However, experimental and simulation results (for approximately $\lambda/2$-spaced arrays) [27], [28] indicate that array responses closely approximating the nominal can be obtained by compensating for the coupling. Thus, adaptive transmit and receive beamforming schemes are expected to automatically compensate for the effect of the coupling within a subarray, without significant loss in beamforming gain.

Anisotropy of antenna elements: While we assume that the elements are isotropic (so that the arrays were free to steer over the range $[0°, 180°]$ in both the polar and azimuthal directions), in reality, the antenna elements will have some directionality, which will limit the steerability of the arrays. In the LOS setting, if the transmitter is at a side wall close to the front of the room, then the horizontal steering angle in the LOS direction approaches $\pm90°$ (since the receiver is at the front wall). When the LOS path is blocked, the optimal horizontal steering angle typically falls in the range $45°$-$75°$, but approaches $90°$ as the transmitter is moved towards the front of the room, regardless of whether or not it is near a side wall. Thus, the horizontal beamwidths of the antenna elements should be chosen to be as large as possible to permit flexibility of placement. Conversely, constraints on the horizontal beamwidths of the individual elements must be taken into account when placing the transceivers. The vertical steering range can typically be narrower. When the LOS is blocked and the transmitter and receiver are very close to each other, the vertical steering angle along the ceiling reflected path does approach $90°$, but the likeihood of blockage presumably will decrease in such a setting.

A. Performance of Waterfilling Benchmark

Fig. 5 depicts how the channel capacity varies as a function of the transmitter's position within the room. Here we have set $N = 2$ and fixed the transmit power per antenna at $P_A = -10$ dBm. The plot can be interpreted as a top-down view of the room with the receiver located at $(2.5, 0)$. The contours at a particular value of (x, y) indicates the channel capacity when the transmitter is located at coordinates (x, y). The capacity is primarily affected by two factors: path loss and spatial correlation. Path loss causes the received signal power, and hence the capacity, to decrease as the transmitter moves farther from the receiver. Spatial correlation fluctuates in a more complex manner based on the link geometry. Given the proposed

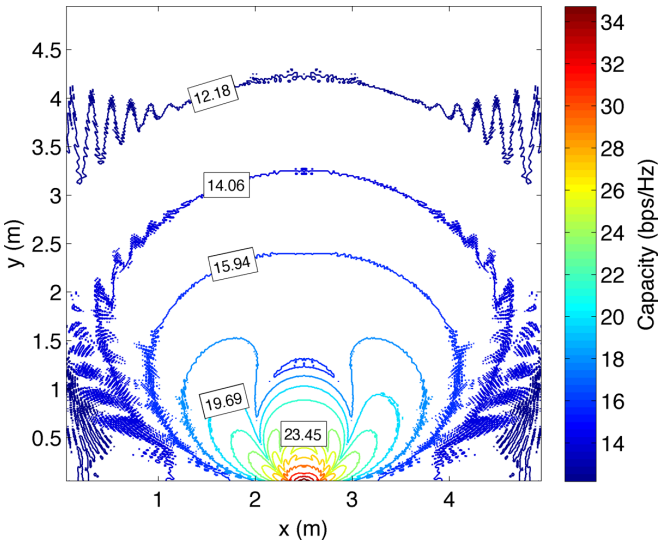

Fig. 5. Channel capacity with waterfilling benchmark scheme as a function of transmitter coordinates.

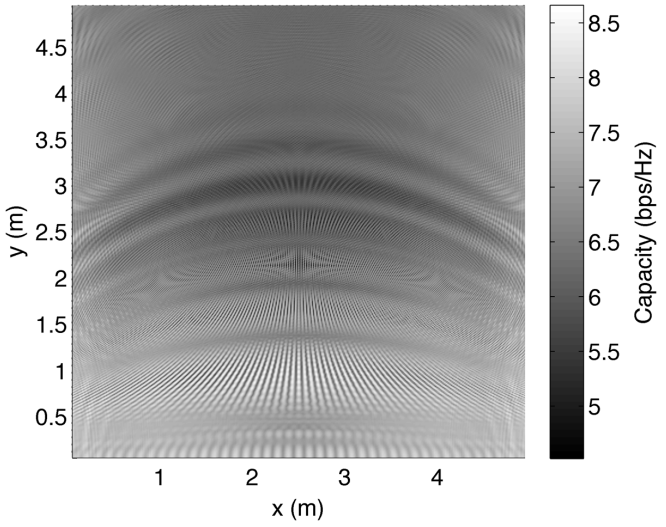

Fig. 6. Channel capacity with waterfilling benchmark scheme assuming LOS blockage.

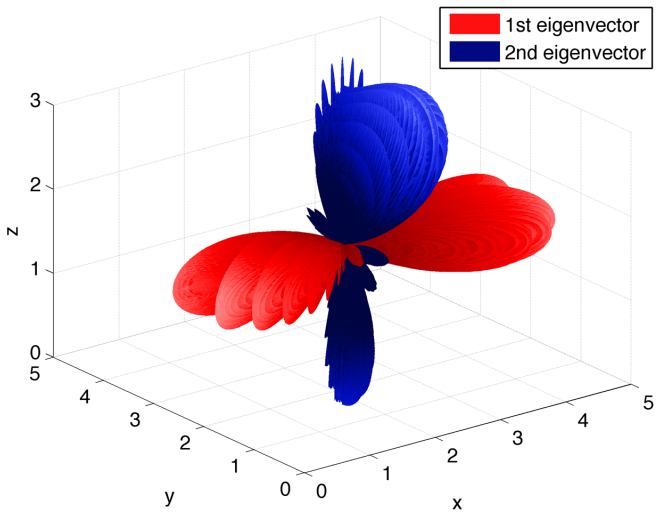

Fig. 7. Transmitter's eigenvector field patterns under LOS blockage scenario when transmit node is located at the center of the room.

architecture, the channel is represented by a 32×32 matrix. We expect two of the thirty-two eigenmodes to be dominant when the spatial correlation between subarrays is low, such as when the transmitter is placed at the center of the room. At this location, the optimal ULA criterion is satisfied. The spatial correlation may increase at other transmitter positions, in which case the second eigenchannel becomes much weaker than the first. As the transmitter moves from the center of the room towards the receiver, for instance, the capacity drops slightly near transmitter coordinates (0, 1.75). This particular fluctuation arises from high correlation in the LOS component of the channel matrix and is independent of the multipath environment.

Fig. 6 plots the capacity as a function of the transmitter's position assuming LOS blockage. Due to the small spatial scale of the capacity fluctuations, a surface plot is used in place of contours. As expected, the absence of the dominant LOS signal component results in lower SNR and capacity throughout the room. In contrast to the LOS scenario, the NLOS channel does not exhibit large fluctuations in capacity due to path loss. Instead, we observe small-scale fluctuations due to variations in spatial correlation. The fluctuations are on the order of several bits/s/Hz and occur over distances on the order of millimeters. This suggests that, especially in NLOS settings, the link must be able to quickly adapt to changes in the transmitter or receiver locations if one or both nodes are mobile.

As described in Section III-A, the left- and right-singular vectors corresponding to the N largest singular values specify the weights of the spatial filters at the receiver and transmitter, respectively. The filters beamsteer in the directions of the N strongest eigenmodes of the channel. In the LOS scenario considered above, both beams are generally directed along the LOS path, which offers the lowest path loss and reflection loss. When the LOS path is blocked, the link must utilize wall and/or ceiling reflections to close the link. In Fig. 7, the radiation patterns produced by the first and second right-singular (transmit) vectors are shown when the transmitter is located in the center of the room. The first eigenvector beamsteers in the directions of the wall reflections, while the second eigenvector utilizes the ceiling reflection. Grating lobes are caused by the subarrays being separated by several wavelengths.

B. Performance of Transmit Beamsteering/Receive MMSE

Fig. 8 plots the spectral efficiency, averaged over random transmitter coordinates, as a function of the per-antenna transmit power P_A. The transmitter's x and y coordinates are taken as independent random variables uniformly distributed over $[0 + L/2, 5 - L/2]$. The performances of both the waterfilling benchmark scheme and the beamsteering/MMSE scheme are included for comparison. In the former case, P_A represents the average transmit power per antenna. In practice, each antenna element would be peak power limited, which is a constraint imposed on the more practical beamsteering/MMSE scheme. We observe that when the constellation is restricted to

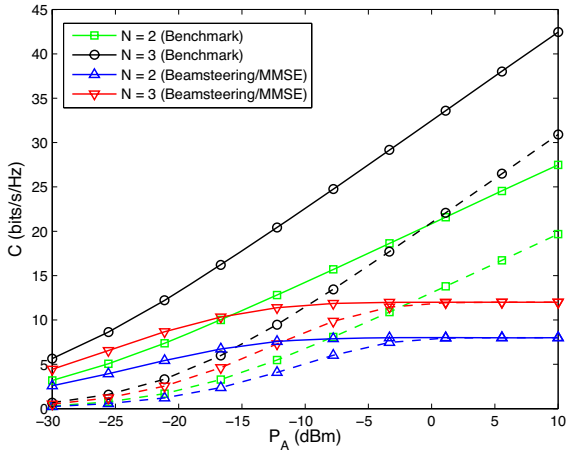

Fig. 8. Channel capacity as a function of P_A, the limit on the average transmit power per antenna. Dashed lines represent the NLOS scenario.

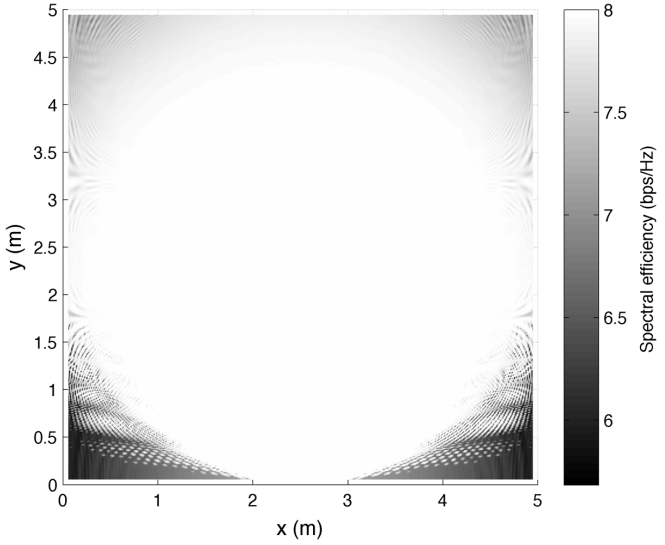

Fig. 9. Channel capacity under transmit beamsteering/receive MMSE scheme.

16-QAM, the spectral efficiency reaches a $4N$ bps/HZ limit as P_A increases. This reduces the impact of LOS blockage on spectral efficiency under the beamsteering/MMSE scheme when the transmit power is sufficiently high.

The spectral efficiency is plotted as a function of transmitter position in Fig. 9 with $N = 2$ and $P = -10$ dBm. The sum-rate capacity approaches the constellation-constrained limit of 8 bps/Hz when the transmitter is placed near the center of the room. Uncoded data can be transmitted at a symbol error rate of $P_e \leq 10^{-5}$ through 85.5% of the room. When the channel is ill-conditioned, such as when the transmitter is placed in one of the front corners of the room, an adaptive link can maintain a low error rate by increasing the transmit power, reducing the constellation size (e.g. QPSK or BPSK), or coding the data symbols. Throughout 86% of the room, the transmitter beamsteers both signals in the direction of the LOS path. In other locations, typically highly correlated locations such as in the front corners of the room, capacity is maximized by transmitting one or both signals along a reflected path.

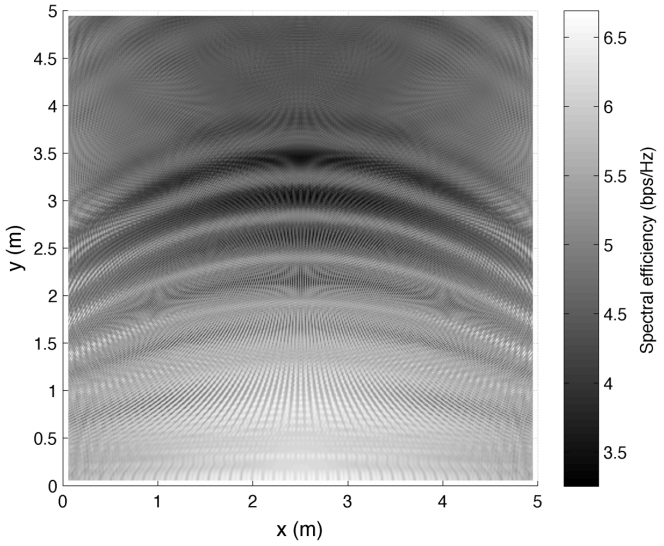

Fig. 10. Channel capacity under transmit beamsteering/receive MMSE scheme.

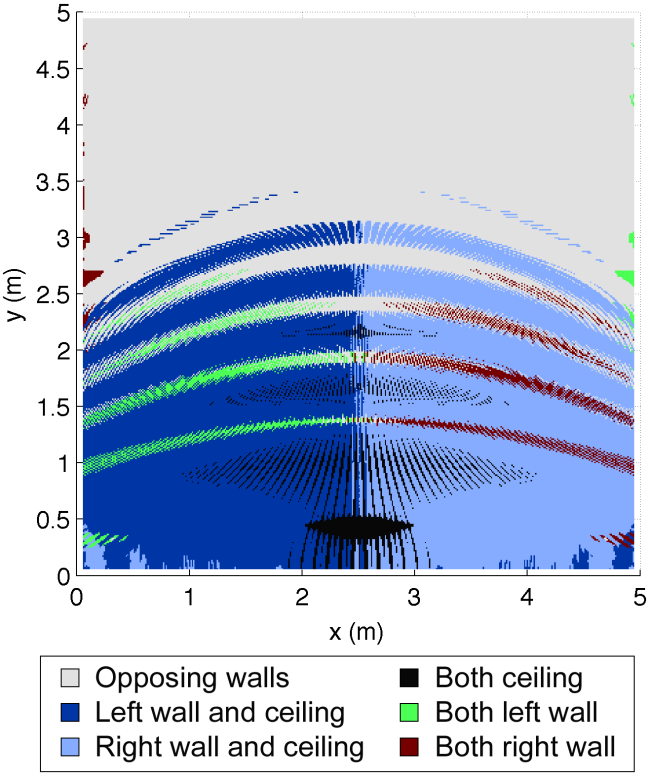

Fig. 11. Capacity-maximizing beamsteering directions when LOS path is obstructed.

When the LOS path is blocked, the spectral efficiency throughout the room varies from 3.2 to 6.5 bps/Hz as shown in Fig. 10. Reliable uncoded transmission at the full 8 bps/Hz rate requires an additional 15 - 20 dBm of power. Alternatively, the transmitter can adapt the coding or modulation scheme to improve link reliability. Fig. 11 plots beamsteering directions that maximize the sum-rate capacity in the NLOS scenario. When the transmitter is located in the back half of the room, for example, the optimal strategy is to steer each subarray towards a different wall reflection. In the front half of the

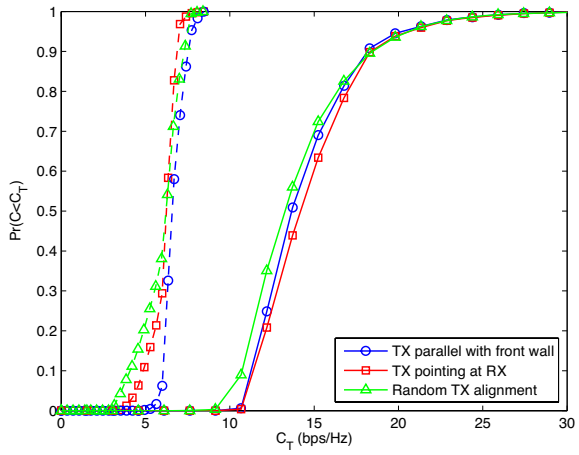

Fig. 12. Cumulative distribution function of the spectral efficiency given various transmitter alignments. Dashed lines represent the NLOS scenario.

room, it is typically optimal to steer one beam towards the ceiling reflection, and the other towards the nearest wall reflection. The remaining schemes of steering both beams towards the ceiling or a single wall are less frequently optimal.

C. Transmitter Alignment

In the previous simulation results, the transmitter is aligned parallel with the front wall. Alternatively, we can consider the scheme where the transmitter is pointed in the direction of the receiver. Fig. 12 compares these two approaches, as well as randomized alignment. We assume $N = 2$ and the waterfilling benchmark scheme is used. The capacity is averaged over the transmitter's x and y coordinates, taken as uniform random variables over $(0, 5)$. We observe from Fig. 12 that aligning the transmitter parallel with the front wall offers the best performance in the NLOS scenario. This occurs because at any given location, the transmitter can beamsteer off either the left or side wall. The second alignment scheme, where the transmitter faces the receiver, offers the best performance when the LOS path is unobstructed. When the LOS path is blocked, however, the near side wall may lie behind the array; as a result, the transmitter must rely on the far wall to provide a reflected path, resulting in higher path loss and lower capacity. Finally, we consider the case where the transmit direction is a uniform random variable chosen in the range $[-90°, 90°]$ with the two extreme values corresponding to the transmitter pointing toward the left and right walls, respectively. Comparing all schemes, we find that the spectral efficiency remains fairly robust to transmitter misalignment.

VI. Conclusions

We have established that spatial multiplexing gains can be layered on top of beamforming gains for indoor 60 GHz links, for nodes whose form factors conform to typical consumer electronics and computing devices. Relating the LOS MIMO channel to prolate spheroidal waveforms, whose eigenvalues drop off sharply around a value related to the array lengths, shows that an array of subarrays architecture is near-optimal: the subarray spacing can be adjusted to provide the maximum number of degrees of freedom for a given form factor, while using multiple antenna elements within a subarray provides beamforming gain and reduces the transmit power per element.

Our simulations indicate that the architecture provides spatial multiplexing gains throughout an indoor environment, and that these gains are robust to node placement and LOS blockage as long as we can electronically steer the beam for each subarray and the horizontal beamwidth of the individual antenna elements is wide enough. For a fixed constellation (which caps the maximum link speed), variations in spectral efficiency due to node placement are reduced. The impact of alignment between the transmitter and receiver arrays, and the geometry of the spatial eigenmodes as a function of node placement and LOS blockage, are discussed. Our promising results motivate future work on extensive performance evaluation for packetized communication with specific coded modulation schemes and signal processing algorithms, and on hardware implementation of the proposed architecture with careful partitioning of analog and digital signal processing.

References

[1] B. Gaucher *et al.*, "Silicon germanium based millimetre-wave ICs for Gbps wireless communications and radar systems," *Semiconductor Science and Technol.*, vol. 22, no. 1, p. S236, 2007.
[2] IEEE Std 802.15.3c-2009 (Amendment to IEEE Std 802.15.3-2003), Oct. 2009.
[3] High Rate 60 GHz PHY, MAC and HDMI PAL, 1st ed., ECMA-387, December 2008.
[4] Wireless Gigabit Alliance. Available: http://wirelessgigabitalliance.org/
[5] WirelessHD. Available: http://www.wirelesshd.org/
[6] I. E. Telatar, "Capacity of multi-antenna Gaussian channels," AT&T Bell Lab Internal Tech. Memo., Oct. 1995.
[7] G. J. Foschini and M. Gans, "On the limits of wireless communications in a fading environment when using multiple antennas," *Wireless Personal Commun.*, vol. 6, no. 3, p. 311, Mar. 1998.
[8] C. Sheldon, M. Seo, E. Torkildson, M. Rodwell, and U. Madhow, "A 2.4 Gb/s millmeter-wave link using adaptive spatial multiplexing," *IEEE Int. AP-S Symp.*, July 2010.
[9] ——, "Four-channel spatial multiplexing over a millimeter-wave line-of-sight link," *IEEE - MTTS International Microwave Symposium*, June 2009.
[10] A. Poon, R. Brodersen, and D. Tse, "Degrees of freedom in multiple-antenna channels: a signal space approach," *IEEE Trans. Inf. Theory*, vol. 51, no. 2, pp. 523–536, Feb. 2005.
[11] D. Gesbert, H. Bolcskei, D. Gore, and A. Paulraj, "Outdoor MIMO wireless channels: models and performance prediction," *IEEE Trans. Commun.*, vol. 50, no. 12, pp. 1926–1934, Dec. 2002.
[12] I. Sarris and A. Nix, "Design and performance assessment of maximum capacity MIMO architectures in line-of-sight," *IEE Proc. Commun.*, vol. 153, no. 4, pp. 482–488, Aug. 2006.
[13] P. Larsson, "Lattice array receiver and sender for spatially orthonormal MIMO communication," in *Proc. IEEE 61st Vehicular Tech. Conf.*, vol. 1, pp. 192–196, May 2005.
[14] F. Bohagen, P. Orten, and G. Oien, "Design of optimal high-rank line-of-sight MIMO channels," *IEEE TRans. Wireless Commun*, vol. 6, no. 4, pp. 1420–1425, Apr. 2007.
[15] H. Xu, V. Kukshya, and T. Rappaport, "Spatial and temporal characteristics of 60-GHz indoor channels," *IEEE J. Sel. Areas Commun.*, vol. 20, no. 3, pp. 620–630, Apr. 2002.
[16] A. Arvanitis, G. Anagnostou, N. Moraitis, and P. Constantinou, "Capacity study of a multiple element antenna configuration in an indoor wireless channel at 60 ghz," in *Proc. IEEE 65th Vehicular Tech. Conf.*, Apr. 2007, pp. 609–613.
[17] E. Torkildson, B. Ananthasubramaniam, U. Madhow, and M. Rodwell, "Millimeter-wave MIMO: wireless links at optical speeds," in *Proc. of 44th Allerton Conference on Communication, Control and Computing*, Sep. 2006.
[18] E. Torkildson, C. Sheldon, U. Madhow, and M. Rodwell, "Nonuniform array design for robust millimeter-wave MIMO links," in *IEEE Global Communications Conference*, Dec. 2009.

[19] F. Bohagen, P. Orten, and G. Oien, "Optimal design of uniform rectangular antenna arrays for strong line-of-sight MIMO channels," *EURASIP J. Wireless Commun. Netw.*, vol. 2007, no. 2, pp. 12–12, 2007.
[20] A. Thaning, P. Martinsson, M. Karelin, and A. T. Friberg, "Limits of diffractive optics by communication modes," *J. Optics A: Pure and Applied Optics*, vol. 5, no. 3, p. 153, 2003. Available: http://stacks.iop.org/1464-4258/5/i=3/a=301
[21] D. Slepian and H. Pollack, "Prolate spheroidal wave functions, Fourier analysis, and uncertainty–I," *Bell Syst. Techn. J.*, vol. 40, pp. 43–63, 1961.
[22] H. J. Landau and H. Pollack, "Prolate spheroidal wave functions, Fourier analysis, and uncertainty–III: the dimension of the space of essentially time and bandlimited signals," *Bell Syst. Techn. J.*, vol. 41, pp. 1295–1336, 1962.
[23] P. F. M. Smulders, "Deterministic modelling of indoor radio propagation at 40-60 Ghz," *Wireless Personal Commun.*, vol. 4, no. 2, pp. 127–135, June 1994.
[24] T. S. Rappaport, *Wireless Communications: Principles and Practice*. Prentice Hall, 2002.
[25] K. Sato, H. Kozima, H. Masuzawa, T. Manabe, T. Ihara, Y. Kasashima, and K. Yamaki, "Measurements of reflection characteristics and refractive indices of interior construction materials in millimeter-wave bands," in *Proc. IEEE 45th Vehicular Tech. Conf.*, 1995, vol. 1, pp. 449–453.
[26] "RO4000® LoPro Laminates data sheet," Rogers Corporation, Chandler, AZ, USA. Available: http://www.rogerscorp.com/documents/1183/acm/RO4000-LoPro-Laminates.aspx
[27] H. Steyskal and J. S. Herd, "Mutual coupling compensation in small array antennas," *IEEE Trans. Antennas Propag.*, vol. 38, no. 12, pp. 1971–1975, Dec. 1990.
[28] Z. Huang, C. A. Balanis, and C. R. Birtcher, "Mutual coupling compensation in ucas: simulations and experiment," *IEEE TRans. Antennas Propag.*, vol. 54, no. 11, pp. 3082–3086, Dec. 2006.

Eric Torkildson received his bachelor's degree in Electrical Engineering from the University of California, San Diego in 2005. He received his master's and Ph.D. degrees from the University of California, Santa Barbara, in 2009 and 2010, respectively. He is currently researching millimeter-wave MIMO communication systems as a staff research associate at UC Santa Barbara.

Upamanyu Madhow is a Professor of Electrical and Computer Engineering at the University of California, Santa Barbara. His research interests are in communication systems and networking, with current emphasis on wireless communication, sensor networks and multimedia security.

He received his bachelor's degree in electrical engineering from the Indian Institute of Technology, Kanpur, in 1985, and his Ph. D. degree in electrical engineering from the University of Illinois, Urbana-Champaign in 1990. He has worked as a research scientist at Bell Communications Research, Morristown, NJ, and as a faculty at the University of Illinois, Urbana-Champaign.

Dr. Madhow is a recipient of the NSF CAREER award. He has served as Associate Editor for the IEEE TRANSACTIONS ON COMMUNICATIONS, the IEEE TRANSACTIONS ON INFORMATION THEORY, and the IEEE TRANSACTIONS ON INFORMATION FORENSICS AND SECURITY. He is the author of the textbook *Fundamentals of Digital Communication*, published by Cambridge University Press in 2008.

Mark Rodwell (B.S., University of Tennessee, Knoxville, 1980, M.S. Stanford University 1982, Ph.D. Stanford University 1988) holds the Doluca Family Endowed Chair in Electrical and Computer Engineering at UCSB. He is Professor and Director of the UCSB Nanofabrication Laboratory and NSF Nanofabrication Infrastructure Network (NNIN), and the SRC Nonclassical CMOS Research Center at the University of California, Santa Barbara. He was at AT&T Bell Laboratories, Whippany, N.J. during 1982-1984. Prof. Rodwell Received the 2010 IEEE Sarnoff Award and the 2009 IEEE IRPM Conference Award for the development of INP-based bipolar IC technology, at both device and circuit design level, for mm-wave and sub-mm-wave applications. His group's work on GaAs Schottky-diode ICs for sub-picosecond / mm-wave instrumentation was awarded the 1997 IEEE Microwave Prize and the 1998 European Microwave Conference Microwave Prize. Prof. Rodwell was elected IEEE Fellow in 2003.